

Variability of sea ice cover in the Chukchi Sea (western Arctic Ocean) during the Holocene

Anne de Vernal and Claude Hillaire-Marcel

Centre de Recherche en Géochimie et en Géodynamique, Université du Québec à Montréal, Montréal, Québec, Canada

Dennis A. Darby

Department of Ocean, Earth, and Atmospheric Sciences, Old Dominion University, Norfolk, Virginia, USA

Received 15 March 2005; revised 8 July 2005; accepted 25 August 2005; published 10 December 2005.

[1] Dinocysts from cores collected in the Chukchi Sea from the shelf edge to the lower slope were used to reconstruct changes in sea surface conditions and sea ice cover using modern analogue techniques. Holocene sequences have been recovered in a down-slope core (B15: 2135 m, 75°44'N, sedimentation rate of ~1 cm kyr⁻¹) and in a shelf core (P1: 201 m, 73°41'N, sedimentation rate of ~22 cm kyr⁻¹). The shelf record spanning about 8000 years suggests high-frequency centennial oscillations of sea surface conditions and a significant reduction of the sea ice at circa 6000 and 2500 calendar (cal) years B.P. The condensed offshore record (B15) reveals an early postglacial optimum with minimum sea ice cover prior to 12,000 cal years B.P., which corresponds to a terrestrial climate optimum in Bering Sea area. Dinocyst data indicate extensive sea ice cover (>10 months yr⁻¹) from 12,000 to 6000 cal years B.P. followed by a general trend of decreasing sea ice and increasing sea surface salinity conditions, superimposed on large-amplitude millennial-scale oscillations. In contrast, $\delta^{18}\text{O}$ data in mesopelagic foraminifers (*Neogloboquadrina pachyderma*) and benthic foraminifers (*Cibicides wuellerstorfi*) reveal maximum subsurface temperature and thus maximum inflow of the North Atlantic water around 8000 cal years B.P., followed by a trend toward cooling of the subsurface to bottom water masses. Sea-surface to subsurface conditions estimated from dinocysts and $\delta^{18}\text{O}$ data in foraminifers thus suggest a decoupling between the surface water layer and the intermediate North Atlantic water mass with the existence of a sharp halocline and a reverse thermocline, especially before 6000 years B.P. The overall data and sea ice reconstructions from core B15 are consistent with strong sea ice convergence in the western Arctic during the early Holocene as suggested on the basis of climate model experiments including sea ice dynamics, matching a higher inflow rate of North Atlantic Water.

Citation: de Vernal, A., C. Hillaire-Marcel, and D. A. Darby (2005), Variability of sea ice cover in the Chukchi Sea (western Arctic Ocean) during the Holocene, *Paleoceanography*, 20, PA4018, doi:10.1029/2005PA001157.

1. Introduction

[2] Observations of the Arctic Ocean during the last decades suggest a decrease in areal extent and thickness of its pack ice [e.g., Johannessen *et al.*, 1999; Vinnikov *et al.*, 1999; Walsh and Chapman, 2001; Comiso, 2002]. This trend can be tentatively attributed to global warming and raises concerns about the stability and fate of the pack ice. It is therefore of primary importance to better document and understand the natural instability and evolution of Arctic pack ice, which cannot be fully assessed from short-term instrumental observations alone, but require analysis of longer time series using geological records. However, the paleoceanography of the Arctic Basin and circum-Arctic seas on centennial to millennial scales is poorly documented because of the rarity of suitable sedimentary records. This is notably due to low sediment accumulation rates at most deep sea locations in the Arctic [e.g., Poore *et al.*, 1999; Backman *et al.*, 2004], which do not permit adequate time

resolution. Moreover, harsh conditions in the surface waters often result in low productivity and biogenic fluxes, and the carbonate and siliceous biological remains are often poorly preserved in the sediment. As a consequence, tracers of past hydrographic changes in the Arctic seas are scarce, and methods most commonly applied to document the paleoceanography of the North Atlantic Ocean, for example, cannot be used unequivocally in the Arctic Ocean. In contrast, organic-walled microfossils or palynomorphs are well preserved in Arctic Ocean sediments and can provide information on past ocean and climate conditions. In particular, the cysts of dinoflagellates (or dinocysts) relating to planktonic production in the surface water layer are useful tracers of sea surface conditions in the arctic and subarctic marine environments [e.g., Mudie *et al.*, 2001]. In the present paper, we report on dinocyst records from cores raised from the shelf edge and the lower slope of the Chukchi Sea (Figure 1). They reveal Holocene sequences with thicknesses ranging from about 10 cm at the deep site (core B15) [Hillaire-Marcel *et al.*, 2004] to more than 200 cm at the shelf site (core P1) [Darby and Bischof, 2004]. In these cores, well preserved dinocyst assemblages permit estimation

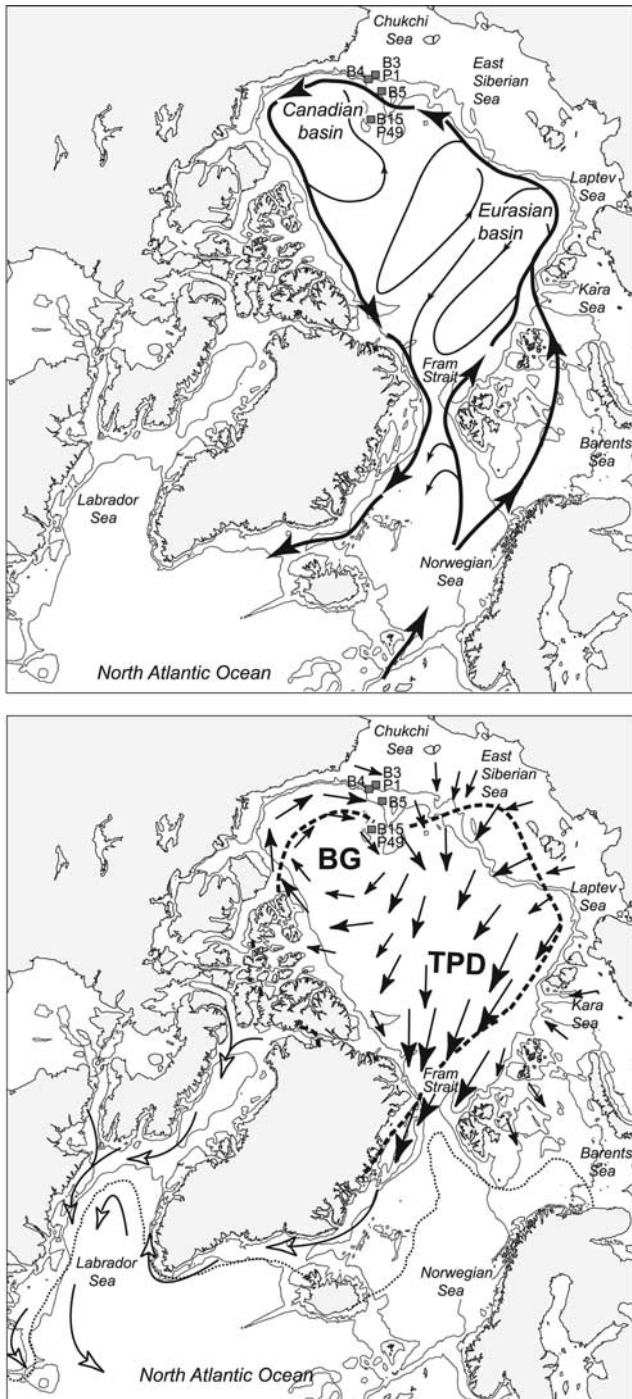


Figure 1. Maps of the Arctic Ocean with the location of the study cores. Isobaths correspond to water depths of 200 and 1000 m. (a) Arrows illustrate the circulation pattern of the North Atlantic Water penetrating into the Arctic Ocean at depths ranging from 200 to 1700 m [cf. Rudels et al., 1994; Jones, 2001]. (b) Main sea ice drifts, the Beaufort Gyre (BG) and the Transpolar Drift (TPD), are schematically shown by black arrows. The main surface currents carrying Arctic sea ice meltwaters toward the North Atlantic are illustrated by open arrows. The maximum (March) and minimum (September) sea ice extents over the Northern Hemisphere are shown by dotted and dashed lines, respectively.

of summer sea surface temperature and salinity, and of the seasonal extent of sea ice cover using modern analogue techniques (MAT) [de Vernal et al., 2001, 2005]. These data, together with information derived from $\delta^{18}\text{O}$ in foraminifer shells from the slope cores [Hillaire-Marcel et al., 2004], provide an insight into the long-term changes in surface to intermediate water masses during the Holocene.

2. Hydrography of the Western Arctic

2.1. Surface and Subsurface Water Masses

[3] The Arctic Ocean, which forms a large polar basin surrounded by lands, can be considered as an enclosed sea. It has limited ocean exchanges with the North Pacific through the shallow (~ 50 m) Bering Strait, but larger connection with the North Atlantic through Fram Strait. These connections impact both the export of low-salinity surface water and sea ice into subarctic basins and the North Atlantic, and the circulation, in the intermediate water layer of the Arctic, of the North Atlantic Water (NAW) (Figure 1a) [Jones, 2001]. This water mass is characterized by temperature and salinity as high as 3°C and 34.5, respectively (Figure 2). In contrast, the uppermost layer is characterized by salinities often below 30 at the surface, as a result of freshwater inputs, notably from Eurasian rivers (Yenisei, Ob, Lena, Kolyma; $\sim 1700 \text{ km}^3 \text{ yr}^{-1}$) and the Mackenzie River ($\sim 260 \text{ km}^3 \text{ yr}^{-1}$) [cf. Carmack, 2000]. As a consequence, the Arctic Ocean is marked by a strong stratification and the existence of a reverse thermocline between the top of the relatively warm intermediate layer originating from the North Atlantic and the base of the cold surface water layer (Figure 2).

2.2. Sea Ice Cover and Ice Drift Patterns

[4] In the Arctic Ocean, sea ice formation occurs largely over the shallow continental shelves surrounding the basin, notably in the East Siberian and Laptev seas, where the shelf is wide and the surface salinity is particularly low because of high freshwater discharge rates from Eurasian rivers [e.g., Barry et al., 1993; Carmack, 2000]. Sea ice spreading northward, toward the central Arctic Ocean, contributes to the development of a multiyear pack ice. Depending upon winds and surface currents, sea ice drifts along two main paths: the Beaufort Gyre, which is a clockwise movement centered in the Canadian Basin, and the Transpolar Drift, which deflects ice away from the Siberian coasts across the Arctic and toward the Atlantic Ocean (Figure 1b). The ice drift velocity ranges generally from 1 to 10 cm s^{-1} , with lower values in the Beaufort Gyre and higher values at the outlet of the Transpolar Drift in the Fram Strait area, which plays a major role with respect to freshwater exports toward the North Atlantic Ocean [e.g., Barry et al., 1993; Dickson et al., 2000; Moritz et al., 2002].

[5] In the Arctic Ocean, the Chukchi Sea seems to be particularly sensitive with regard to sea ice since a large reduction in ice concentration has been observed in its shelf area from the 1980s to the 1990s [cf., e.g., Comiso, 2002]. This recent change in the Chukchi Sea ice could be the result of reduced sea ice production on this shelf, more summer ice melting, because of warmer surface waters and/

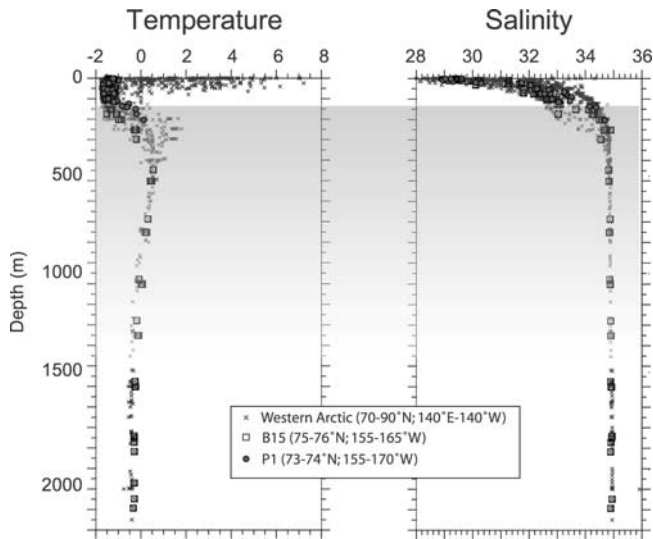


Figure 2. Temperature and salinity versus depth in the water column of the western Arctic Ocean (grey symbols correspond to measurements between 140°E and 140°W and from 70° to 90°N) and around coring sites (B15, blue symbols; P1, red symbols). The data are from the Goddard Institute database (available at <http://www.giss.nasa.gov/data/o18data/> [cf. Schmidt, 1999; Bigg and Rohling, 2000]). The grey horizon corresponds to the North Atlantic water mass below the cold and low-saline surface Arctic water layer. See color version of this figure at back of this issue.

or change in the relative strength and position of the Beaufort Gyre versus the Transpolar Drift.

3. Material and Methods

3.1. Coring Sites and Chronology of the Sedimentary Sequences

[6] This study is based on the analysis of cores collected on the edge of the continental shelf of the Chukchi Sea and on the lower slope of the adjacent Northwind Basin. These cores were initially sampled in order to study the flux of sediment and nutrients from the shelf into the basin as part of the Shelf-Basin-Interaction Project [Darby *et al.*, 2001]. The box core AR-92-B15 (B15) was collected at 2135-m water depth on the lower slope. This core, as well as others from the Northwind Basin (see core P49; Figure 1), is characterized by very low sedimentation rates, of the order of centimeters per kiloyears, but it contains relatively abundant calcareous foraminifers allowing isotopic measurements [Poore *et al.* 1999; Hillaire-Marcel *et al.*, 2004]. On the upper slope, sedimentation rates are much higher, but calcareous foraminifers are extremely rare and do not permit continuous isotope measurements. Piston core AR-92-P1 (P1) and the associated box core AR-92-B3 (henceforth referred to as P1/B3) are from the shelf edge, in 201 m water depth, and contain more than 200 cm of Holocene sediments.

[7] Despite low sedimentation rates, core B15 is particularly interesting because it yields both calcareous microfossil assemblages and palynological assemblages. An initial

study was conducted on core B15 using a continuous sampling of 1-cm-thick slices. The isotopic data in planktonic and benthic foraminifers and the chronology based on three AMS ^{14}C dates from foraminifers are reported by Hillaire-Marcel *et al.* [2004]. The ages converted to calendar years based on Calib 4.0 [Stuiver *et al.*, 1998] indicate very low sedimentation rates, with a sequence of about 10 cm spanning the entire Holocene. Taking into account the biological mixing of sediment (unpublished lead 210 measurements suggest mixing in the top centimeter, decreasing down to 3 cm [cf. Hillaire-Marcel *et al.*, 2004]), each slice of one cm represents about 1000 years. A second study of the box core was undertaken in order to improve the sampling resolution. The archived core B15 was entirely sampled at 0.5-cm interval, and the chronology of the initial working core has been used after point to point correlations based on palynological data. These correlations indicate that the surface 2 cm of sediment are better represented in the archive core B15, whereas the lower part has been condensed. The ^{14}C chronology we used here results from calibration with Calib 5.0 [Stuiver and Reimer, 1993] based on the calibration data set of Hughen *et al.* [2004] (see Table 1). The ages are almost identical to those reported by Hillaire-Marcel *et al.* [2004]. In both cases the calibration was made after a reservoir correction of 750 years (i.e., $\Delta R = 350$ years), which would account for the regional air-sea $^{14}\text{CO}_2$ difference in the Canadian Arctic [cf. Mangerud and Gulliksen, 1975; Blake, 1987]. A reservoir correction larger in the Canadian Basin than in the Eurasian Basin is consistent with the mean age of the water that suggest less ventilated water masses in the western Arctic than in the eastern Arctic [Jutterström and Anderson, 2005].

[8] The chronostratigraphy of cores P1 and B3 collected on the Chukchi shelf was established using AMS ^{14}C dates on mollusk shells and a mixed population of benthic foraminifers [cf. Darby and Bischof, 2004]. Seven dates were obtained in core P1, and four in core B3 (see Figure 3 and Table 1). The overlap in ^{14}C ages, ^{210}Pb measurements and a detrital dolomite peak in both cores show that 20 cm of sediment is missing from the top of core P1 and that approximately 5 cm are also missing on top of core B3 because of overpenetration of the box corer. Despite some missing material at the sediment water interface, the composite sequence of cores P1 and B3 yields a sedimentary record representative of most of the Holocene interval. In order to develop an age model, we evaluated the calibrated ages with Calib 5.0 after a reservoir correction of 750 years (i.e., $\Delta R = 350$ years) as we did for core B15 (see *supra*). The interpolation between dates suggests variable sedimentation rates ranging from 6.5 to 60 cm kyr^{-1} . Core B3 is characterized by a sedimentation rate of about 35 cm kyr^{-1} . The analyses of 1-cm-thick slices at 1-cm interval down to 30 cm provide a multidecadal chronological resolution for the 200- to 1000-year interval. In the upper 70 cm of core P1, much lower sedimentation rates (down to 6.5 cm kyr^{-1}) are recorded. The analyses performed at 3-cm intervals on average yield a centennial time resolution for the interval spanning 5000 to 1000 cal years B.P. In the lower part of core P1, corresponding to the early Holocene, a few ^{14}C measurements indicate sedimentation rates as high as 60 cm kyr^{-1} .

Table 1. Radiocarbon Ages Used to Develop Age-Depth Models^a

Core	Depth, cm	Equivalent Middle Depth, cm	Material Dated	¹⁴ C Date Normalized	Calibrated Age		
					$\Delta R = 0$	$\Delta R = 250$	$\Delta R = 350$
AR-92-B3	0–1	0.5	mixed benthic foraminifers	940 ± 70	540	330	240
AR-92-B3	12–13	12.5	mollusc fragments	1230 ± 50	770	560	500
AR-92-B3	25–26	25.5	mollusc fragments	1530 ± 30	1080	850	720
AR-92-B3	41–42	41.5	mollusc fragments	1980 ± 30	1540	1270	1200
AR-92-P1	24–26	45 ^b	mollusc fragments	2170 ± 90	1760	1500	1360
AR-92-P1	49–51	70 ^b	mollusc fragments	3340 ± 50	3190	2840	2770
AR-92-P1	64–66	85 ^b	mixed benthic foraminifers	5120 ± 110	5500	5130	5040
AR-92-P1	99–100	119.5 ^b	mixed benthic foraminifers	6240 ± 70	6680	6170	6315
AR-92-P1	105	125 ^b	<i>Bathyarca</i> sp.	6590 ± 70	7100	6750	6695
AR-92-P1	134–136	155 ^b	mixed benthic foraminifers	7030 ± 110	7510	7310	7210
AR-92-B15	0–1	2.5 ^c	<i>N. pachyderma</i>	3800 ± 50	3719	3445	3337
AR-92-B15	5–6	5.5 ^c	<i>N. pachyderma</i>	6485 ± 50	6988.5	6695	6576
AR-92-B15	11–12	8.5 ^c	<i>N. pachyderma</i>	10710 ± 80	12098	11552	11329

^aRadiocarbon ages given in years B.P.

^bDepth corrected taking into account 20 cm missing at the top of the core.

^cEquivalent depth in the archive core.

Age versus depth extrapolation below 135 cm indicate that the base of the palynological record at 240 cm in core P1 should not be older than 10,000 years.

3.2. Reconstruction of Sea Ice Cover Extent, Sea-Surface Salinity, and Temperature Based on Dinocysts

[9] The hydrographical estimates are principally based on the analyses of organic-walled dinoflagellate cyst assemblages that are well preserved in the sediment, and represent an important part of both autotrophic and heterotrophic planktonic production. A number of recent studies dealing with dinocyst assemblages in surface sediments of arctic and subarctic seas have demonstrated their close relationships with sea surface parameters such as summer temperature, salinity, and seasonal extent of sea ice cover [Mudie, 1992; Kunz-Pirrung, 1998, 2001; Mudie and Rochon, 2001; Voronina et al., 2001; Radi et al., 2001; de Vernal et al., 2001, 2005]. On these grounds, transfer functions using the modern analogue techniques (MAT) have been developed [de Vernal et al., 2001, 2005].

[10] The reconstruction of sea surface conditions presented here is based on a recently updated dinocyst database that includes 60 taxa and 1054 reference sites from middle to high latitude of the North Atlantic and North Pacific oceans, the Arctic Ocean and adjacent subpolar seas (see Figure 4). Hydrographic estimates are calculated from a set of five modern analogues selected in the reference database after neperian logarithmic transformation of the relative abundances of taxa in the assemblages. The hydrographic data used as input for the reconstructions were compiled for a radius of 30 nautical miles around each site from the 2001 version of the *National Ocean Data Center* [2001] atlas. Sea ice data were compiled on a 1° by 1° grid scale from the 1953–2000 data set provided by the National Snow and Ice Data Center (NSIDC) in Boulder (Colorado). Sea ice cover is expressed here in terms of months per year with sea ice concentration greater than 50%. It is a parameter that correlates with the mean annual sea ice concentration, but which is slightly more sensitive to small sea ice cover values (see Figure 5).

[11] Hydrographic data compiled in the NODC-2001 atlas are very rare for the Arctic region. This, adding to large

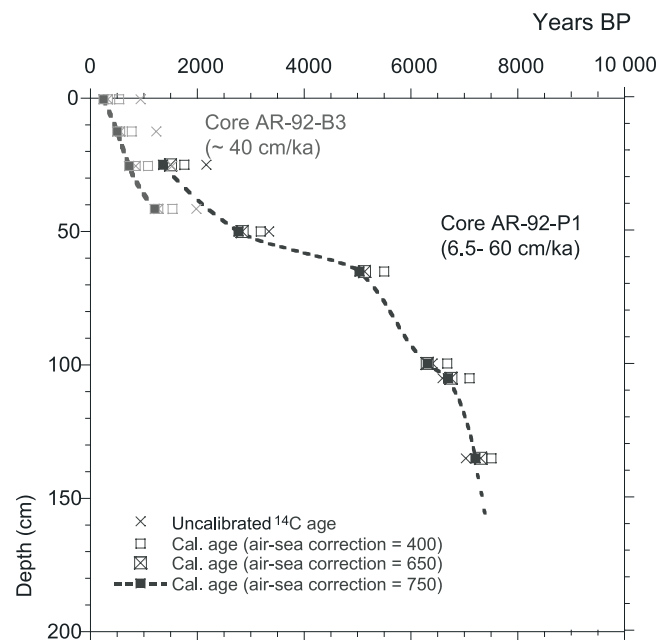


Figure 3. Age versus depth relationship in cores P1 and B3 according to AMS ¹⁴C dates on mollusk shells or mixed benthic foraminifer populations (see Table 1). The dates were calibrated using the Calib 5 software [Stuiver and Reimer, 1993] and the marine calibration data set of Hughen et al. [2004] after normalization for a $\delta^{13}\text{C}$ of -25‰ and correction for the air-sea carbon reservoir effect by subtracting 400 years ($\Delta R = 0$), 650 years ($\Delta R = 250$), or 750 years ($\Delta R = 350$). In the present study, we are using calibrated ages after a correction of 750 years, which would account for the regional air-sea CO_2 reservoir difference [cf. Mangerud and Gulliksen, 1975; Blake, 1987]. The age model is based on an interpolation between the dates and suggests variable sedimentation rates ranging from 6.5 to 60 cm kyr⁻¹.

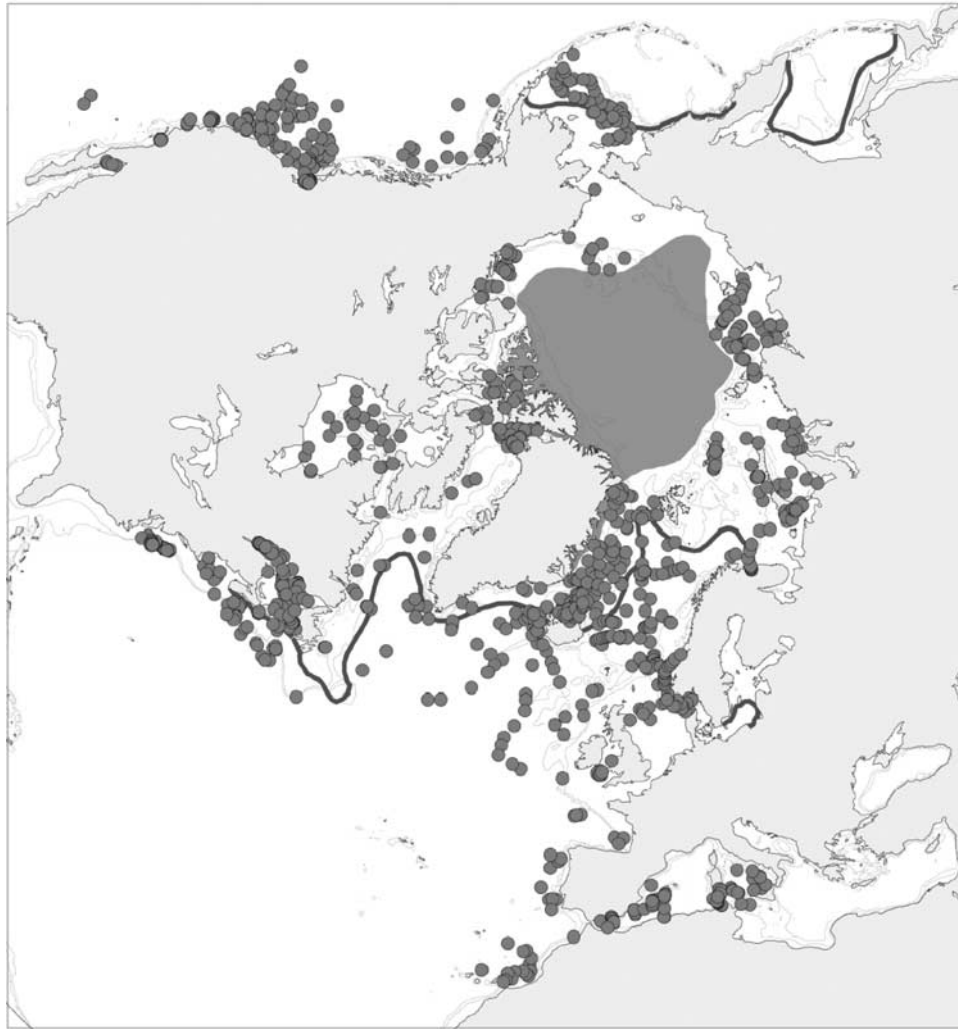


Figure 4. Map showing the location of surface sediment samples used to develop the reference dinocyst database ($n = 1054$). The minimum and maximum sea ice cover extents are shown by the blue zone and the blue line, respectively. The database includes assemblages for 516 sites characterized by seasonal sea ice, about half of them corresponding to more than 6 months per year of sea ice. It is important to mention that many other samples collected under the perennial pack ice of the Arctic Ocean revealed barren assemblages. These samples are not included in the database. In the Arctic Ocean context, barren dinocyst assemblages are associated with nil cyst fluxes because of extremely low productivity. See color version of this figure at back of this issue.

interannual variations in temperature and salinity of surface waters of the Arctic seas, introduces some uncertainties in the reconstruction of past conditions. Nonetheless, the use of the modern analogue technique with the dinocyst database still permits the quantitative reconstruction of past sea surface conditions with a reasonable degree of accuracy. The overall error of prediction calculated from modern assemblages is $\pm 1.6^{\circ}\text{C}$ for the temperature of August, and ± 1.2 for the salinity. It is of note that these errors are close to the actual standard deviation around the mean for the summer temperature and salinity data, which average 1.6°C and 1.1, respectively. The overall error of prediction for the reconstruction of sea ice is ± 1.2 months yr^{-1} for the $>50\%$ sea ice cover, which is also equivalent to the mean

standard deviation around the average for modern ice coverage.

3.3. ^{13}C and ^{18}O Signals of Foraminifer

[12] Planktonic foraminifers are present in sufficient number in the postglacial section of core B15, which was collected on the slope, to permit stable isotope analysis in distinct size fractions. In cores B3 and P1, collected on the shelf in relatively shallow waters (~ 200 m), planktonic foraminifers are very rare and isotopic measurements could not be performed. The absence or rarity of planktonic foraminifers from the shelf sediments is probably due to the deep dwelling behavior of *Neogloboquadrina pachyderma*, which dominates almost exclusively the

assemblages. In arctic and subarctic basins, shell growth and/or secondary calcite overgrowth of *N. pachyderma* generally occur at the depth of the summer pycnocline [e.g., Kohfeld et al., 1996], and its ^{13}C and ^{18}O contents are size and weight (density) dependent [Hillaire-Marcel et al., 2004]. Two varieties are observed, one left-coiled (Npl), one right-coiled (Npl). In view of their identical isotopic properties, they are thought to represent the two varieties of the same “cryptic” species of *N. pachyderma* [see Darling et al., 2000; Bauch et al., 2003]. In the western Arctic, the assemblages are depleted by nearly 3‰ in $\delta^{18}\text{O}$ with respect to values of a calcite precipitated in equilibrium with ambient waters. However, the data also show a negative relationship between the shell weight (or size) and its ^{18}O content ($-0.15 \pm 0.03\text{‰} \mu\text{g}^{-1}$), whereas the ^{13}C content shows a positive correlation with mean shell weight ($+0.12 \pm 0.01\text{‰} \mu\text{g}^{-1}$) [cf. Hillaire-Marcel et al., 2004]. In surface sediments, the reverse shell weight versus $\delta^{18}\text{O}$ relationship has been attributed to the reverse temperature gradient, along the thermocline, between the cold and dilute surface water layer and the more saline subsurface North Atlantic Water mass, almost 3°C warmer (see Figure 2). Thus, despite offsets with equilibrium conditions, the reverse size-weight versus $\delta^{18}\text{O}$ relationship in planktonic foraminifers from the western Arctic seems to be a response to temperature gradients along the pycnocline. A similar pattern of general offset with equilibrium conditions, but a preserved temperature-gradient dependence, has been observed in *Globigerina bulloides* during in vitro growth experiments [Spero and Lea, 1996]. The isotopic composition in Npl shells picked from different size fraction can thus be used a proxy for temperature gradients between the surface and subsurface water layers. In addition to planktonic foraminifers, we have performed measurements on one benthic foraminiferal species (*Cibicides wuellerstorfi*), which provides complementary information on bottom water conditions.

4. Results: Postglacial Paleoceanographic Records

4.1. Record From the Lower Slope

[13] The upper part of core B15 contains well preserved foraminifers and dinocysts that permit to establish an isotope stratigraphy and to reconstruct sea surface conditions (Figures 6 and 7), whereas the interval below 11 cm is barren of both calcareous and organic-walled microfossils. This lower interval, which should be older than 15,000 cal years B.P. according to linear extrapolation of the few ^{14}C dates (Figure 7), probably corresponds to extremely harsh conditions with permanent pack ice. Generally low productivity and extremely harsh conditions before termination 1 in the Eurasian Basin of the central Arctic Ocean were also inferred from ostracod fauna [Cronin et al., 1995].

[14] In the upper 11 cm of core B15, the dinocyst assemblages are characterized by concentrations ranging 10^2 – 10^3 cysts cm^{-3} and by a relatively low diversity of species. Taking into account sedimentation rates of the order of 1 cm kyr^{-1} , one may calculate fluxes on the order of 10^{-1} – 10^0 cysts $\text{cm}^2 \text{ yr}^{-1}$. Such low cyst fluxes, together

with low diversity of species, reflect cold conditions and a generally low productivity on the average (Figure 6). The assemblages are dominated by two autotrophic taxa *Operculodinium centrocarpum* and/or *Pentapharsodinium dalei*, which are ubiquitous in high-latitude environments. In the modern database of dinocysts, established from the analyses of surface sediment samples, the quasi-exclusive occurrence of these taxa is observed in extremely cold polar environments [de Vernal et al., 2001, 2005]. In view of the ubiquitous distribution of *O. centrocarpum* and *P. dalei*, it is worth mentioning that it is the low diversity and composition of the assemblages that indicate cold conditions rather than the ecology of the species.

[15] A higher diversity of species and significant occurrence of accompanying taxa such as *Impagidinium pallidum*, *Spiniferites elongatus* and *S. ramosus* in many samples suggest slightly milder conditions in surface waters during the intervals where *O. centrocarpum* is somewhat lower in abundance (Figure 6).

[16] A particular feature of the dinocyst assemblages in core B15 is the almost exclusive occurrence of cysts belonging to the Gonyaulacales and the rarity of Protoperidinales, such as *Brigantedinium* and *Islandinium*. Because these taxa are more sensitive to oxidation [e.g., Marret, 1993; Zonneveld et al., 2001], their low occurrence might result from a selective degradation of organic matter fostered by low burial rates and low carbon fluxes to the seafloor. Alternatively, the low fluxes of Protoperidinales, which are heterotrophic and feed on diatoms, may be associated with low pelagic productivity in an environment characterized by extensive sea ice cover. Multivariate analyses of the spatial distribution of dinocyst taxa in surface sediment of the North Atlantic, Arctic, sub-Arctic and North Pacific have shown a close relationship between Protoperidinales and productivity, which is dominated by diatoms in high-latitude marine environments [cf. Devillers and de Vernal, 2000; de Vernal et al., 2001; Radi et al., 2001; Radi and de Vernal, 2004; Hamel et al., 2002]. We thus interpret the sparse occurrence of *Brigantedinium* and *Islandinium* in the assemblages of core B15 as a response to low planktonic production, which is consistent with low concentration of benthic and planktonic foraminifers in sediments of the deep Arctic Ocean [e.g., Osterman et al., 1999] and with biochemical measurements in the water column indicating low carbon fluxes to the seafloor [Jutterström and Anderson, 2005]. In any case, the dinocyst database includes many assemblages from the Arctic seas with various proportions of *Brigantedinium* or *Islandinium*. Therefore, even if we cannot rule out totally the possibility of selective degradation in surface sediments or in down-core samples, the set of modern dinocyst data permits sea surface reconstruction with a high degree of confidence, especially since the sea surface conditions estimated here are based on close analogues in the modern data set.

[17] Qualitative interpretation as well as quantitative estimates based on MAT indicates extremely cold conditions in surface waters, with some warming phases marked by near ice-free conditions for a few months per year (Figure 7). These oscillations appear significant with respect to the maximum and minimum possible values reconstructed, and

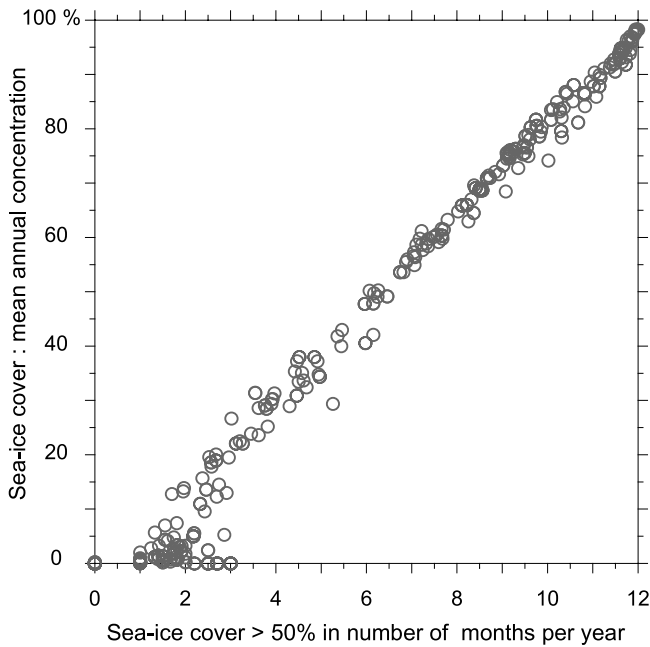


Figure 5. Sea ice cover data in the reference database used for estimating sea surface condition from dinocyst assemblages. The number of sites is 1054, many of which from arctic and subarctic seas being representative of dense sea ice cover (see Figure 4). The data from 1953 to 2000 are compiled from the National Snow and Ice Data Center for a 1° by 1° grid scale. They can be expressed either in terms of mean annual concentration or in terms of months per year of sea ice cover.

also because their amplitude exceeds the degree of uncertainty of the approach. On the basis of the sea surface condition estimates, dinocyst concentration, and isotopic composition of foraminifers, the succession of distinct episodes can be identified as described here.

[18] 1. The occurrence of dinocysts indicative of an autotrophic production suggests that ice-free conditions prevailed for a few weeks to a few months per year as early as 15,000 cal years B.P. An early postglacial episode dated between about 14,000 and 12,000 cal years B.P. was marked by an early warming with a sea ice cover of less than 10 months yr^{-1} . This interval is also marked by the occurrence of a few foraminifer shells, and by a slight depletion in the $\delta^{18}\text{O}$ record of *Neogloboquadrina pachyderma* left coiling.

[19] 2. From about 12,000 to 10,000 cal years B.P., biogenic fluxes were low. Dinocyst data indicate the recurrence of extremely cold conditions with close to 12 months yr^{-1} of sea ice, whereas maximum $\delta^{18}\text{O}$ values are recorded in both planktonic and benthic foraminifers. Although it seems a little too young, this interval could be tentatively associated with the Younger Dryas episode [cf. also Hillaire-Marcel et al., 2004] in view of the chronological uncertainties in core B15.

[20] 3. After about 10,000 cal years B.P., there is a sharp transition marked by significant dinocyst concentration

increase, the beginning of a warming trend of surface waters in summer, the occurrence of both varieties of *Neogloboquadrina pachyderma* (right and left coiled), and an important shift in $\delta^{18}\text{O}$ values toward lighter values of both planktonic and benthic foraminifers. This transition corresponds to the major shift between glacial and interglacial conditions.

[21] 4. An early Holocene episode, spanning about 9000 to 7000 years B.P. is characterized both by maximum dinocyst concentrations and a slight warming of surface waters. Despite extensive sea ice cover, this episode was marked by optimum temperature conditions in subsurface waters (> 200 m) as shown by much lighter $\delta^{18}\text{O}$ values in large size planktonic foraminifers. Particularly large isotopic gradients are then observed between small-size and large-size *Neogloboquadrina pachyderma* shells (both left and right coiled [see Hillaire-Marcel et al., 2004]), indicating an important change in the structure of the upper water column, with an enhanced stratification of the surface water layer over a warmer subsurface North Atlantic Water mass. On the basis of the isotopic data from the initially studied core B15, Hillaire-Marcel et al. [2004] proposed that the North Atlantic subsurface water mass was about 4°C at the study site, which is 3°C warmer than at present. It is of note that dinocyst data from the Laptev Sea and slope also suggest warmer temperature conditions and maximum inflow of North Atlantic waters during the early Holocene [Matthiessen et al., 2001; Polyakova et al., 2005]. Micro-paleontological and isotopic data from the Northwind Basin as well as from the Eurasian margins of the Arctic Ocean therefore indicate an inflow rate of the North Atlantic Water significantly higher during the early Holocene than at present and/or enhanced warming of this water mass along its North Atlantic pathway, possibly in response to the early Holocene maximum insolation at 60°N .

[22] 5. The interval following 7000 cal years B.P. is marked by reduced isotopic gradients between small-size and large-size *Neogloboquadrina pachyderma* shells, which suggest a decrease in the vertical gradient of temperature and a lesser stratification between the surface and subsurface water masses. This interval is also characterized by large variations in sea ice cover, with episodes of reduced sea ice extent also marked by a higher summer temperature (up 5°C) and higher salinity (up to 32), alternating with harsher intervals. The record of sea surface conditions therefore reflects changes in the stratification of water masses, with reduced sea ice episodes resulting from more vertical mixing and a lesser stratified surface water layer. Three episodes of reduced sea ice extent are recorded at about 6000, 4000 and 2500 cal years B.P.

4.2. Record From the Shelf Edge

[23] The other Holocene record is obtained from the composite time series combining data from core B3 and nearby piston core P1 (Figures 8 and 9). At this coring site, the planktonic foraminiferal content is very sparse but dinoflagellate cysts are relatively abundant with a concentration range of 10^3 – 10^4 cysts cm^{-3} (Figure 8). Taking into account sedimentation rates of the order of 20 cm kyr^{-1} , one may calculate fluxes on the order of 10^1 – 10^2 cysts $\text{cm}^2 \text{yr}^{-1}$,

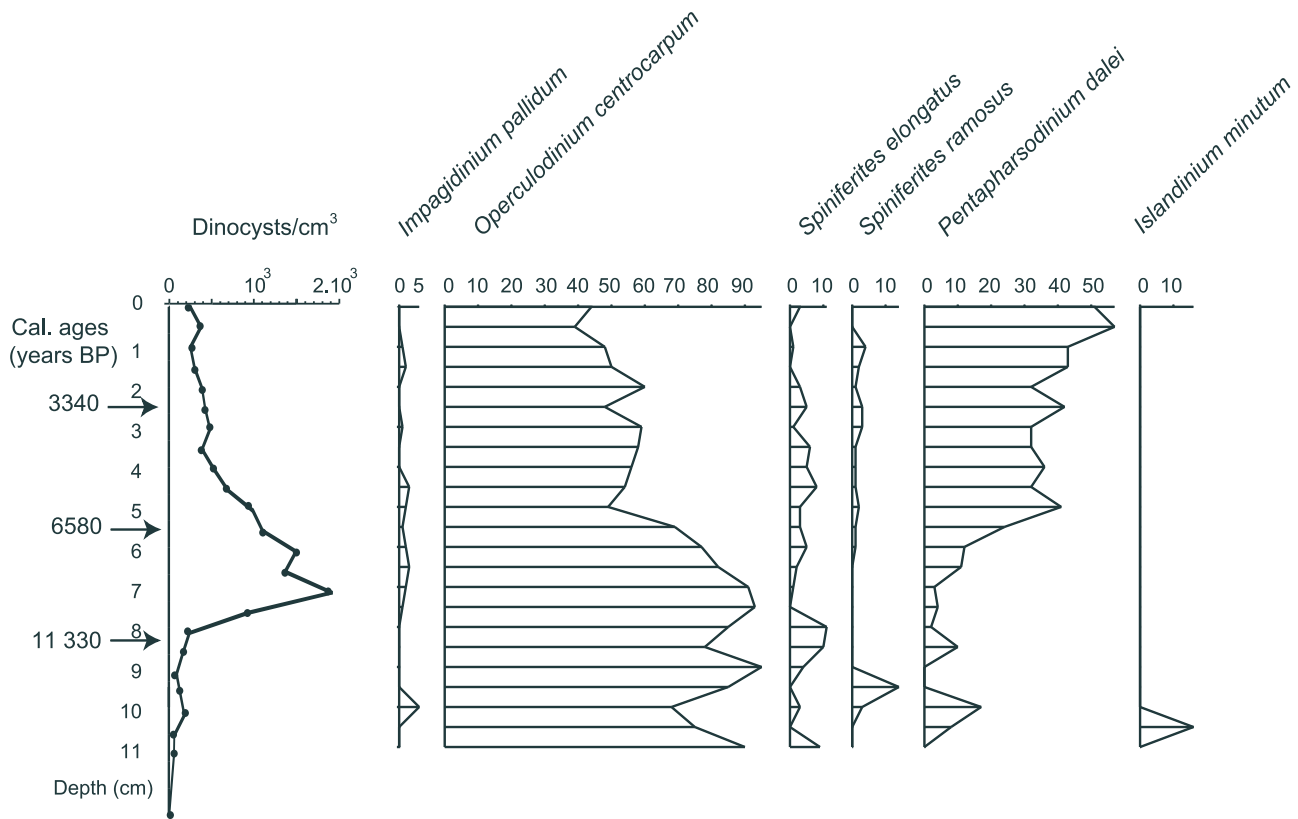


Figure 6. Diagram of dinocyst concentration and percentages in the archive core B15. The calibrated radiocarbon dates are transferred from the initial working core B15 [cf. *Hillaire-Marcel et al.*, 2004] (see Table 1).

which reflect productivity higher by 1 to 3 orders of magnitude than that of the slope core B15.

[24] As in core B15, the dinocyst assemblages are characterized by high percentages of *O. centrocarpum* and *P. dalei* (Figure 8). Moreover, as in core B15, the relative abundance of *O. centrocarpum* decreases toward the top of the core, whereas the proportion of *P. dalei* increases. This trend seems thus to have a regional ecostratigraphical significance. Beyond these general features, the dinocyst record of cores P1 and B3 differs from that of core B15 in having a higher diversity of species and different composition of assemblages with regard to secondary taxa. In contrary to core B15, *S. ramosus* and *I. pallidum* occur sporadically, and *S. elongatus* records lower percentages. Furthermore, taxa related to a heterotrophic production are common. They include *Brigantidinium* spp., *Islandinium minutum* and *Islandinium? cezare*. As mentioned in section 4.1, in the modern distribution of dinocysts, these taxa appear characteristic of high-productivity arctic and subarctic areas, such as estuaries, shelf environments or polynyas, where diatoms are abundant and constitute suitable preys for heterotrophic dinoflagellates [e.g., *Hamel et al.*, 2002; *Radi et al.*, 2001].

[25] The dinocyst assemblages permit quantitative reconstruction of sea surface conditions which show important fluctuations (Figure 9). However, it is difficult to assess the frequency of these fluctuations and to distinguish noise from significant changes on millennial or centennial scales.

This limitation is notably due to the large changes in sedimentation rates (from 6.5 to 60 cm kyr⁻¹) that result in different time slices represented by the samples. Nevertheless, despite uncertainties in the chronological resolution of some sections of the record, a few points can be raised.

[26] 1. The assemblages indicate consistently warmer than present conditions, with a summer temperature oscillating between 4°C and 7°C throughout most of the sequence, compared to modern SST near 0°C. The absolute values of the temperature can be discussed, but the assemblages and temperature estimate show well above freezing condition in surface waters during the summer season.

[27] 2. The reconstructions suggest large amplitude salinity variations, generally between 25 and 30. Beyond short (century scale) oscillations, the record shows possibly significant lower frequency (millennial scale) changes. A phase of relatively high salinity (up to 33) at the base of the sequence is followed by a sudden decrease to less than 25 at about 8000 cal years B.P. From about 8000 to 3000 cal years B.P., salinity remained low and then increased above 28 between 3 and 2 ka. The high-resolution, subcentennial, record of the core B3 also suggests high-frequency salinity variations superimposed on a decreasing trend of salinity from about 1200 to 200 cal years B.P.

[28] 3. The Holocene dinocyst data in P1/B3 indicates seasonally ice-free conditions and a highly variable sea ice

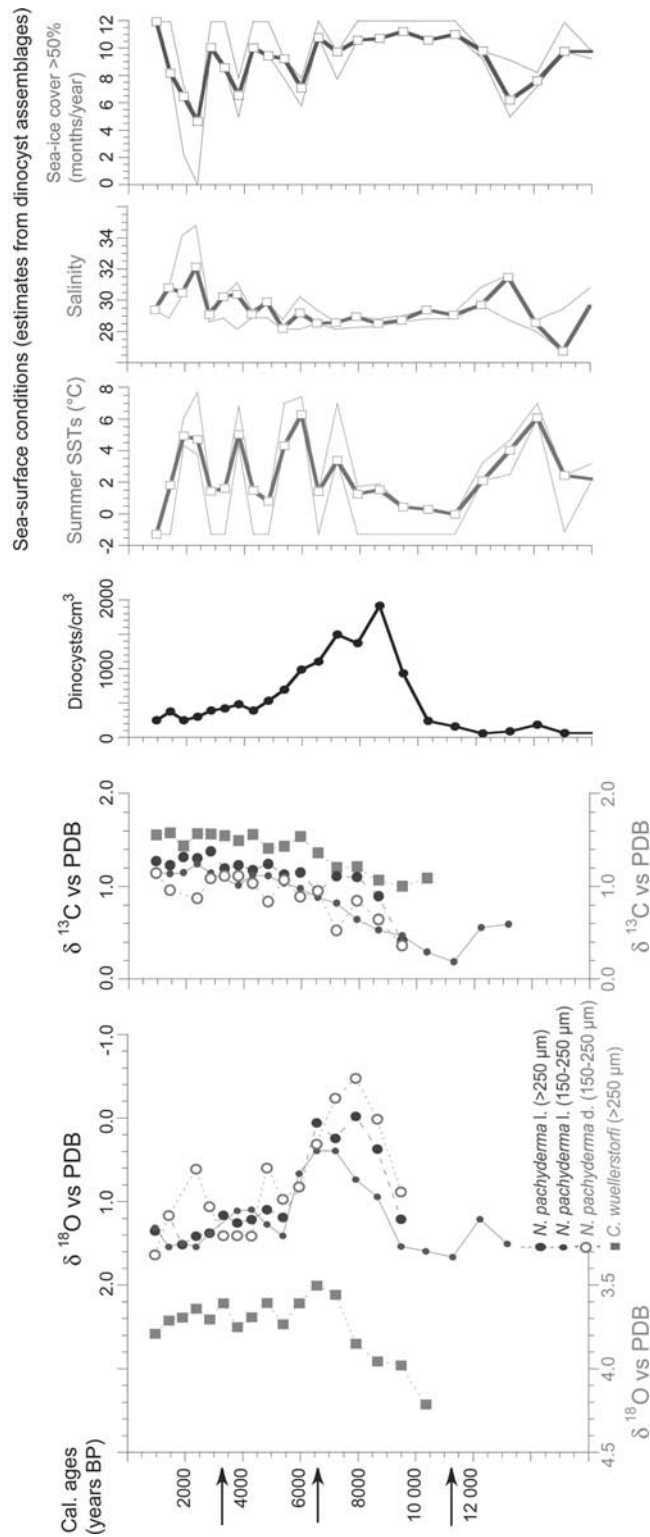


Figure 7. Isotopic data ($\delta^{18}\text{O}$ and $\delta^{13}\text{C}$) of benthic and planktonic foraminifer shells hand-picked in different size fractions, dinocyst concentrations, and estimates of sea surface conditions based on dinocyst assemblages in the archive core B15. The squares correspond to the best estimates, which are the averages weighted inversely to the distance for the five best modern analogues (for details, see *de Vernal et al.* [2001]). The thin lines correspond to the minimum and maximum values possible according to the set of five analogues. The vertical scale is the calibrated age as interpolated from the three age controls shown by arrows. See color version of this figure at back of this issue.

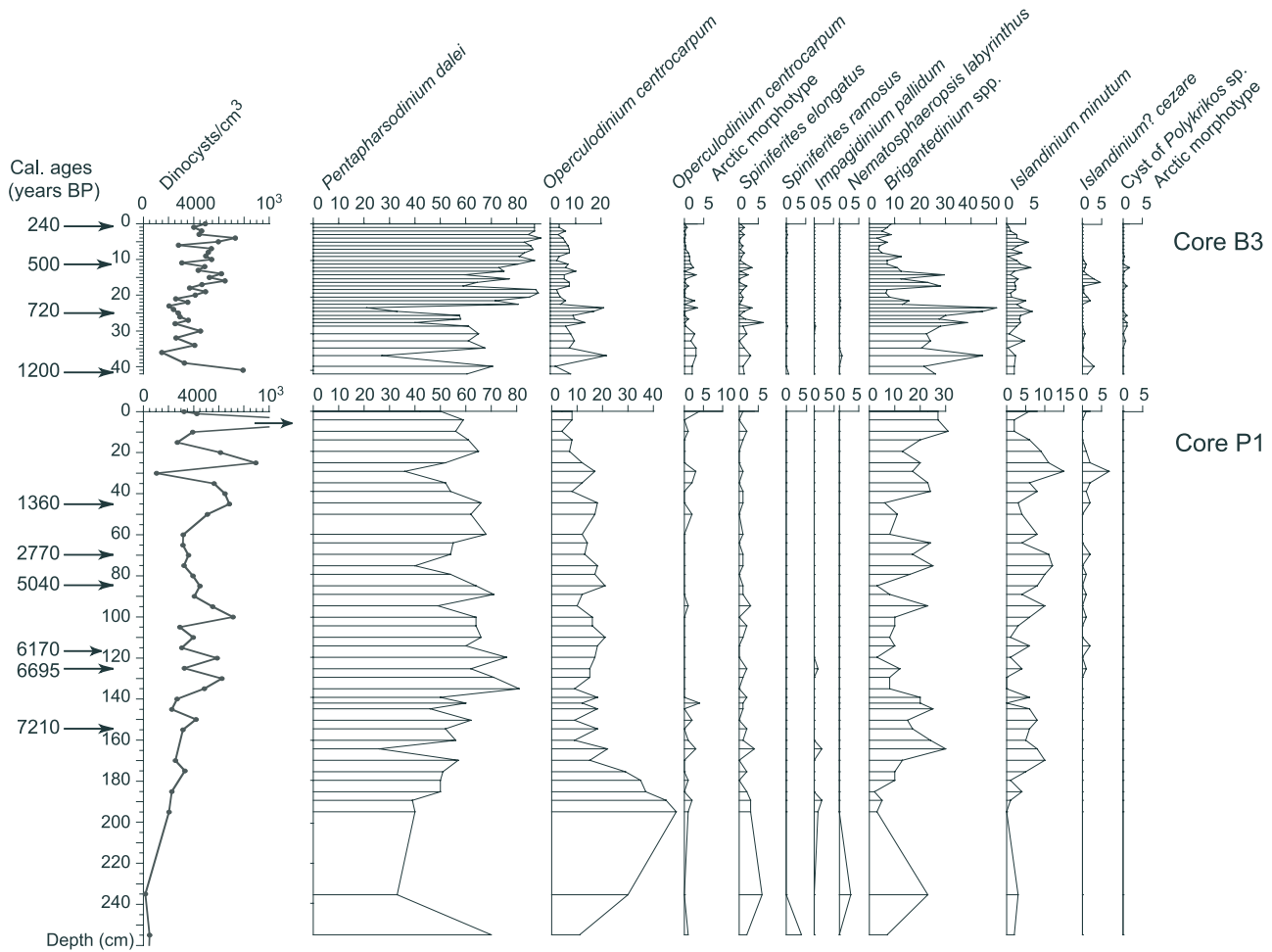


Figure 8. Diagram of dinocyst concentrations and percentages in cores B3 and P1.

cover, ranging from 2 to 12 months yr^{-1} . Minimum sea ice is reconstructed for the base of the sequence and maximum at the top. Beyond the large amplitude high-frequency oscillations, three phases with particularly reduced extent of sea ice are identified: before 8000 cal years B.P., at about 6000 cal years B.P. and between 3000 and 2000 cal years B.P. The coarse silt and sand fractions that relate to melting at the sea ice margin and release of entrained sea ice sediment [Hebbeln and Wefer, 1991] provides complementary information on sea ice cover and drift patterns [Darby, 2003; Darby and Bischof, 2004]. It suggests higher inputs than at present during most of the Holocene, notably around 2500 and 6000 cal years B.P., and before 8000 cal years B.P., thus indicating enhanced sea ice rafting and melting, and warmer conditions during a longer ice-free season (Figure 9). Thus the coarse silt and sand fractions as well as dinocyst records yield a consistent picture of sea ice cover variations at the edge of the Chukchi shelf during the Holocene.

5. Discussion

5.1. Sea Ice Variations

[29] The two Holocene records of sea ice variations presented here contain time series with different chronolog-

ical resolution. The shelf edge record (cores B3 and P1) permits recognition of oscillations with multidecadal to centennial frequencies, whereas the resolution of the slope record (B15) cannot resolve higher than multimillennial frequencies.

[30] On average, the reconstructions indicate colder conditions and more extensive sea ice cover at the slope site (B15) located closer to the pole than at the shelf site (P1/B3). The amplitude of sea ice fluctuations seems also to be larger on the shelf than offshore, which can be due to the higher sedimentation rates and lesser temporal smoothing of the shelf record. Higher sensitivity of the shelf environments with respect to sea ice formation and hydrographical conditions could also be evoked [cf. Weingartner *et al.*, 2005]. This sensitivity was probably larger during the early Holocene, when eustatic sea level was lower and the Arctic shelves more exposed than today [e.g., Bauch *et al.*, 2001; W. F. Manley, Postglacial flooding of the Bering Land Bridge: A geospatial animation: INSTAAR, University of Colorado, v1, http://instaar.colorado.edu/QGISL/bering_land_bridge, 2002, hereinafter referred to as Manley, Bering Land Bridge animation, 2002]. The important changes recorded in coarse silt-sand fraction and sea ice cover at about 8000 cal years B.P. in the shelf core P1 coincide with the end of the postglacial transgression in the

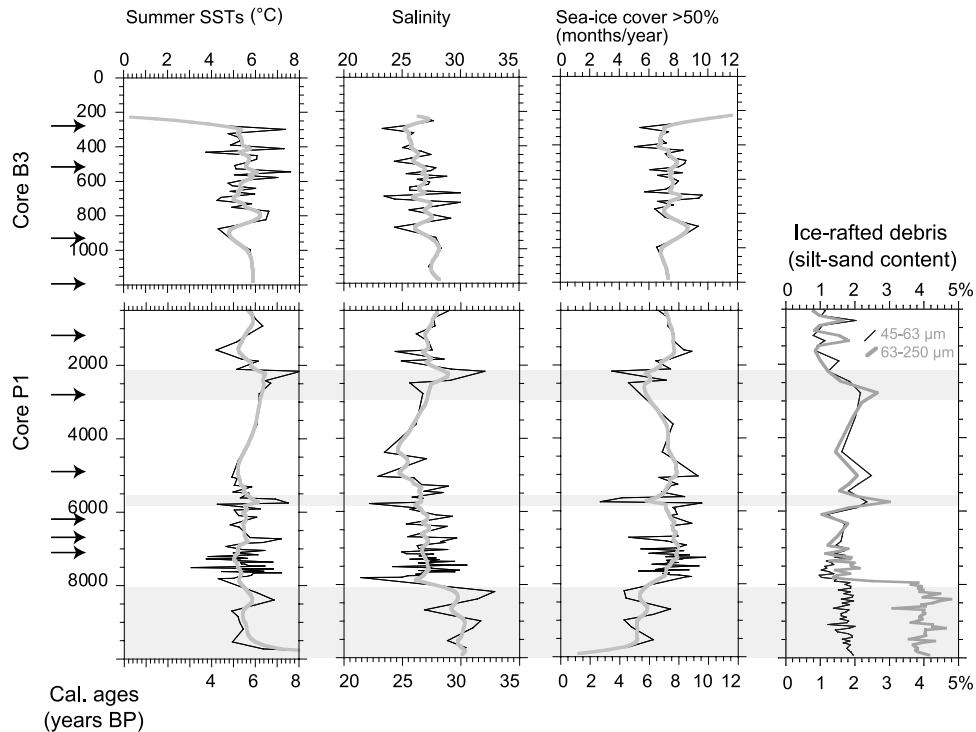


Figure 9. Estimates of sea surface conditions based on dinocyst assemblages in cores B3 and P1. Only the best estimates are illustrated in Figure 9. These estimates consist of averages weighted inversely to the distance for the five best modern analogues (for details, see *de Vernal et al.* [2001]). The thick lines correspond to three-point running averages. At the right the silt and sand fraction in percentage against the dry weight is shown as a complementary indication of summer ice melt. The vertical scale is the calibrated age, as interpolated from age control points shown by arrows for the interval spanning the last 7200 years. Below, the ages are extrapolated, and there is a large uncertainty in the chronology.

Arctic, prior to the stabilization of sea level close to its present limit in the Chukchi shelf area [*Mason and Jordan*, 2002; *Manley*, Bering Land Bridge animation, 2002]. Therefore the transition recorded in sea surface conditions and sediment in core P1 at about 8000 years B.P. could be a response to a change in the bathymetry and regional physiography rather than a direct response to large-scale climate change. In other words, the shelf core record probably reflects the early Holocene sea level rise, as also observed in Laptev Sea records [e.g., see *Polyakova et al.*, 2005].

[31] The sea surface condition records of cores P1/B3 and B15 are difficult to compare because of the different bathymetric settings, but show a few consistent features. Both records indicate less extensive sea ice than at present during most of the Holocene. They also show significant variations, beyond the degree of uncertainty of the approach. Moreover, in contrast with many high-latitude records of climate changes, they do not provide clear evidence for an early-to-middle Holocene thermal optimum, when summer insolation was higher than at present. On the contrary, data of core B15 suggests extensive sea ice cover for more than 10 months yr^{-1} during an interval spanning about 12,000 to 6000 cal years B.P., with peaks of minimum sea ice before 12,000 cal years B.P. and after 6000 cal years B.P. These features are very interesting from a hemispheric paleoclimate point of view because they present some

convergence with apparent anomalies in the terrestrial postglacial records of vegetation and climate changes over the western Arctic [*Kaufman et al.*, 2004]. Indications for a very early thermal optimum prior to 11,500 cal years B.P. are found in lakes of the northern Bering Strait area and peat deposits on the Chukchi Shelf [*Elias et al.*, 1992, 1996; *Anderson*, 1988; *Ager*, 2003], with a climate deterioration paradoxically starting when summer insolation at 60°N reached its maximum [cf. *Kaufman et al.*, 2004]. This early thermal optimum, which is a peculiarity of the northern Bering Strait area, is consistent with the early peak of minimum sea ice and maximum sea surface temperature recorded in core B15. Ice free and relatively warm sea surface conditions in summer, together with larger shelf area exposed during the early postglacial may explain the regional thermal optimum of the northern Bering Strait area, whereas enhanced sea ice after 12,000 cal years B.P. at site B15 might be involved as a factor linked to subsequent regional cooling.

[32] In a similar manner, the sea ice extent has been evoked as a key factor to explain the asymmetric distribution of biomes in circum Arctic regions some 6000 years ago [*Kaufman et al.*, 2004]. As shown in a comprehensive compilation of mid-Holocene paleovegetational data from high latitudes of the Northern Hemisphere, the western Arctic region shows little paleovegetational differences, when compared with the modern. It shows a tree limit

similar to the present one in Beringia, whereas, in Eurasia, pollen data indicate significantly warmer conditions and a much more northern position of the tree line [Bigelow *et al.*, 2003]. Data-model comparisons for the mid-Holocene indicate that the most realistic simulations are obtained with climate model experiments including sea ice dynamics, which result in similar ice thickness in the western Arctic, but reduced sea ice in the eastern Arctic [Vavrus and Harrison, 2003; Kaufman *et al.*, 2004]. In the 6000 years B.P. experiment, which is a “warming” experiment with insolation forcing, models with sea ice dynamics show that sea ice thins rapidly in areas of ice divergence such as the shelves of the Eurasian Arctic, and much less rapidly in areas of sea ice convergence [cf. Hewitt *et al.*, 2001; Vavrus and Harrison, 2003]. In the western sector of the Arctic, sea ice convergence results in minimum change in ice concentration for the 6000 years B.P. simulation, leading in turn to a low surface air temperature anomaly in Alaska and the Canadian Arctic, when compared with the eastern subarctic regions, which were then significantly warmer [Kaplan *et al.*, 2003; Vavrus and Harrison, 2003].

[33] Core B15 data suggest more unstable sea ice conditions after about 6000 cal years B.P., with millennial-scale oscillations in the ice extent. Periods of minimal sea ice are recorded at about 6000, 4000, and 2000 cal years B.P., which could be related to changes in the strength or pattern of the main drift at the origin of sea ice convergence in the western Arctic [cf. Darby and Bischof, 2004]. Alternatively, variations in sea ice may result from changes in the structure of the halocline, which depends upon precipitation and freshwater runoff in the Arctic [e.g., Weatherly and Walsh, 1996]. A weaker stratification fosters ocean heat fluxes toward the surface and thus sea ice melting. Reduced episodes of sea ice cover off the Chukchi shelf could therefore correspond to a weaker ice drift and/or a weaker halocline because of lesser freshwater inputs, whereas phases with enhanced sea ice would correspond to a stronger drift and/or to a sharper stratification because of higher freshwater inputs. In the modern climate, the Transpolar Drift strength and pattern, and the precipitation over the Arctic, are positively related to the Arctic Oscillation (AO) and North Atlantic Oscillation (NAO) [Dickson *et al.*, 2000; Mysak, 2001; Peterson *et al.*, 2002; Rigor *et al.*, 2002; Moritz *et al.*, 2002]. Thus it is entirely possible that a link exists between the decadal to millennial variability of sea ice cover in the western Arctic and the relative frequencies of the atmospheric circulation patterns similar to the AO-NAO modes.

5.2. Stratification of the Upper Water Masses

[34] The record of core B15 includes data from the photic zone (dinocysts) and from the top of the subsurface layer (planktonic foraminifers). It thus permits inferences about stratification of the upper water column and the buoyancy of the surface water layer. The isotope data in planktonic foraminifers clearly show an early Holocene optimum in subsurface temperature peaking around 8000 cal years B.P. This optimum has been attributed to enhanced inflow and/or a warmer North Atlantic Water flowing into the Arctic [Hillaire-Marcel *et al.*, 2004]. Evidence for significantly

warmer conditions during the early Holocene, at the northern end-member of the North Atlantic Drift (NAD), can be found from sea surface temperature reconstruction in the Norwegian Sea [Andersen *et al.*, 2004], and from subsurface foraminifer data (assemblages and/or isotopic composition) in the Barents Sea [Duplessy *et al.*, 2001; Sarnthein *et al.*, 2002] and west of Spitsbergen [Hald *et al.*, 2004]. The Barents Sea records as well as data from the Chukchi Sea records indicate maximum northward inflow of North Atlantic waters contributing to the gyres in the subsurface water layer of the Arctic Ocean (see Figure 1a). Paradoxically, this early Holocene optimum in subsurface waters corresponds to maximum sea ice cover at the surface in the study area. It also corresponds to a minimum in the estimated sea surface salinity, which therefore suggests the existence of a very sharp stratification with a strong halocline in the upper water column.

[35] The opposite response of the subsurface versus surface water layers is reduced after 6000 years B.P. Isotope data in planktonic foraminifers show a decrease in the temperature of the North Atlantic Water and/or its inflow rate. This transition coincides with a trend toward an increase in sea surface salinity and a reduced extent of sea ice cover, thus suggesting a weaker halocline fostering heat transfer from the subsurface to the surface of the water column. The millennial-scale oscillations that seem to characterize the sea surface conditions after 6000 years B.P. could be related to variations in the water mass stratification and vertical mixing, possibly because of changes in freshwater inputs to the Arctic. Holocene changes in precipitation over the Russian Arctic were proposed on the basis of pollen data [e.g., Andreev and Klimanov, 2000; Andreev *et al.*, 2001], oxygen isotope data in cellulose [Wolfe *et al.*, 2000], and marine sedimentological data allowing paleoriver runoff estimates [Stein *et al.*, 2004]. The various precipitation-related curves presented by Stein *et al.* [2004] and Andreev *et al.* [2001] illustrate millennial to centennial oscillations that cannot be correlated with the sea ice cover or salinity in the western Arctic because of poor chronological resolution in the later case. Nevertheless, they all show decreasing trends in both precipitation and river discharge since 6000 years, which is consistent with an increased sea surface salinity and could moreover explain a decline in sea ice production over the Russian Arctic shelves.

6. Conclusion

[36] The western Arctic (Chukchi Borderland) is a critical region for monitoring sea ice production and extent because it is located in a convergence zone between the Beaufort gyre and the Transpolar Drift, which plays a major role in Arctic sea ice export toward the North Atlantic [e.g., Aagaard and Carmack, 1989; Hilmer *et al.*, 1998], thus on the buoyancy of surface waters in the western Nordic seas and the Labrador Sea, where deep and intermediate waters of the North Atlantic form today [e.g., Marshall and Schott, 1999]. Sea ice in the western Arctic is, however, a complex function. It relates to sea ice production, which takes place mainly in the Russian seas and depends upon the

surface salinity, stratification and winter cooling. It also relates to the spreading of newly formed sea ice toward the west central Arctic Ocean depending upon the strength and position of the Transpolar Drift. Moreover, the radiative and thermal forcing play a role on sea ice melting and sea ice budget. In view of the high interannual variability in sea ice thickness observed during the last decade, it is difficult to assess the respective importance of the different mechanisms involved [e.g., Laxon *et al.*, 2003]. The sea ice reconstructions in the Chukchi Sea presented here shed some light on the mechanisms that apparently dominate the long-term Holocene record. First, the sea ice record does not follow the summer insolation pattern over high latitudes, demonstrating that the radiative forcing did not exert as such the most determinant role on the sea surface conditions of the western Arctic during the Holocene. Second, the decoupling between subsurface and sea surface conditions together with sea surface salinity estimates suggest that stratification is a determinant parameter, possibly driven by precipitations over the Arctic and Eurasia. Third, paleoclimatic data provide evidence for strong meridional heat flux from the North Atlantic to the Arctic via the atmosphere (see terrestrial climate records) or through subducting NAD waters (see marine records), which point toward early Holocene conditions similar to those of strongly positive AO modes described from the modern climatology. These include poleward shift of the Transpolar Drift, increased production of ice over the Eurasian Arctic

shelves, enhanced divergence in the eastern Arctic resulting in positive temperature anomalies and reduced summer sea ice, as well as convergence in the western Arctic, resulting in negative temperature anomalies in the Beaufort Sea and little summer sea ice change in the Western Arctic [cf. Rigor *et al.*, 2002]. Finally, sea ice data appear coherent with the results of mid-Holocene coupled model simulations in which a “dipole pattern” is distinguished on the basis of sea ice anomaly distribution showing an opposition between the eastern and western Arctic [e.g., Vavrus and Harrison, 2003].

[37] The importance of sea ice has been emphasized as an amplifier or “switch” in the climate system [e.g., Gildor and Tziperman, 2000]. From a western Arctic perspective, it seems that the Arctic sea ice is also critical with respect to the bipolar character of climate that shows an opposition between the east and the west, not only in the Arctic, but possibly also in the northern North Atlantic [Hillaire-Marcel *et al.*, 2001; Solignac *et al.*, 2004].

[38] **Acknowledgments.** This study is a contribution to project GR-240 of the Canadian Foundation for Climate and Atmospheric Sciences and to the western Arctic Shelf Basin Interaction project in (NSF grant OPP-9817051). Initial funding by the Climate System History and Dynamics project supported by the Natural Sciences and Engineering Research Council of Canada is also acknowledged. The support in the laboratory of Julie Leduc and Maryse Henry, both from GEOTOP, has been essential. We are grateful to the reviewers, Jens Matthiessen and Thomas Cronin, for their careful examination of the manuscript and their constructive comments.

References

- Aagaard, K., and E. C. Carmack (1989), The role of sea ice and other freshwater in the Arctic circulation, *J. Geophys. Res.*, *94*(C10), 14,485–14,498.
- Ager, T. A. (2003), Late Quaternary vegetation and climate history of the central Bering Land Bridge from St. Michael Island, western Alaska, *Quat. Res.*, *60*, 19–32.
- Andersen, C., N. Koç, A. Jennings, and J. T. Andrews (2004), Nonuniform response of the major surface currents in the Nordic Seas to insolation forcing: Implications for the Holocene climate variability, *Paleoceanography*, *19*, PA2003, doi:10.1029/2002PA000873.
- Anderson, P. M. (1988), Late Quaternary pollen records from the Noatak and Kobuk River drainages, northwestern Alaska, *Quat. Res.*, *29*, 263–267.
- Andreev, A. A., and V. A. Klimanov (2000), Quantitative Holocene climatic reconstruction from Arctic Russia, *J. Paleolimnol.*, *24*, 81–91.
- Andreev, A. A., V. A. Klimanov, and L. D. Sulerzhitsky (2001), Vegetation and climate history of the Yana River lowland, Russia, during the last 6400 yr, *Quat. Sci. Rev.*, *20*, 259–266.
- Backman, J., M. Jakobsson, R. Løvlie, L. Polyak, and L. A. Febo (2004), Is the central Arctic Ocean a sediment starved basin?, *Quat. Sci. Rev.*, *23*, 1435–1454.
- Barry, R. G., M. C. Serreze, J. A. Maslanik, and R. H. Preller (1993), The Arctic sea ice-climate system: Observations and modeling, *Rev. Geophys.*, *31*, 397–422.
- Bauch, D., K. Darling, J. Simstich, H. A. Bauch, H. Erlenkeuser, and D. Kroon (2003), Palaeoceanographic implications of genetic variation in living North Atlantic *Neoglobobadrina pachyderma*, *Nature*, *424*, 299–302.
- Bauch, H. A., T. Mueller-Lupp, E. Taldenkova, R. F. Spielhagen, H. Kassens, P. M. Grootes, J. Thiede, J. Heinemeier, and V. V. Petryashov (2001), Chronology of the Holocene transgression at the north Siberian margin, *Global Planet. Change*, *31*, 125–139.
- Bigelow, N. H., et al. (2003), Climate change and Arctic ecosystems: 1. Vegetation changes north of 55°N between the Last Glacial Maximum, mid-Holocene, and present, *J. Geophys. Res.*, *108*(D19), 8170, doi:10.1029/2002JD002558.
- Bigg, G. R., and E. J. Rohling (2000), An oxygen isotope data set for marine water, *J. Geophys. Res.*, *105*, 8527–8535.
- Blake, W., Jr. (1987), Geological Survey of Canada radiocarbon dates XXVI, *Pap. Geol. Surv. Can.*, *87–7*, 60 pp.
- Carmack, E. C. (2000), The Arctic Ocean’s freshwater budget: Sources, storage and export, in *The Freshwater Budget of the Arctic Ocean*, edited by E. L. Lewis *et al.*, pp. 91–126, Springer, New York.
- Comiso, J. C. (2002), Correlation and trend studies of the sea ice cover and surface temperatures in the Arctic, *Ann. Glaciol.*, *34*, 420–428.
- Cronin, T. M., T. R. Holtz Jr., R. Stein, R. Spielhagen, D. Fütterer, and J. Wollenburg (1995), Late Quaternary paleoceanography of the Eurasian Basin, Arctic Ocean, *Paleoceanography*, *10*, 259–281.
- Darby, D. A. (2003), Sources of sediment found in sea ice from the western Arctic Ocean, new insights into processes of entrainment and drift patterns, *J. Geophys. Res.*, *108*(C8), 3257, doi:10.1029/2002JC001350.
- Darby, D. A., and J. F. Bischof (2004), A Holocene record of changing Arctic Ocean ice drift analogous to the effects of the Arctic Oscillation, *Paleoceanography*, *19*, PA1027, doi:10.1029/2003PA000961.
- Darby, D. A., J. Bischof, G. Cutter, A. de Vernal, C. Hillaire-Marcel, G. Dwyer, J. McManus, L. Osterman, L. Polyak, and R. Poore (2001), New record shows pronounced changes in Arctic Ocean circulation and climate, *Eos Trans. AGU*, *82*(49), 601, 607.
- Darling, K. F., C. Wade, I. A. Stewart, D. Kroon, R. Dingle, and A. J. Leigh Brown (2000), Molecular evidence for genetic mixing of Arctic and Antarctic subpolar populations of planktonic foraminifers, *Nature*, *404*, 43–47.
- de Vernal, A., et al. (2001), Dinoflagellate cyst assemblages as tracers of sea-surface conditions in the northern North Atlantic, Arctic and sub-Arctic seas: The new “n = 677” database and application for quantitative paleoceanographical reconstruction, *J. Quat. Sci.*, *16*, 681–699.
- de Vernal, A., et al. (2005), Reconstruction of sea-surface conditions at middle to high latitudes of the Northern Hemisphere during the Last Glacial Maximum (LGM) based on dinoflagellate cyst assemblages, *Quat. Sci. Rev.*, *24*, 897–924.

- Devillers, R., and A. de Vernal (2000), Distribution of dinocysts in surface sediments of the northern North Atlantic in relation with nutrients and productivity in surface waters, *Mar. Geol.*, *166*, 103–124.
- Dickson, R. R., T. J. Osborn, J. W. Hurrell, J. Meincke, J. Blindheim, B. Adlandsvik, T. Vinje, G. Alekseev, and W. Maslowski (2000), The Arctic Ocean response to the North Atlantic Oscillation, *J. Clim.*, *13*, 2671–2696.
- Duplessy, J.-C., E. Ivanova, I. Murdmaa, M. Paterne, and L. Labeyrie (2001), Holocene paleoceanography of the northern Barents Sea and variations in the northward heat transport of the Atlantic Ocean, *Boreas*, *30*, 2–16.
- Elias, S. A., S. K. Short, and R. L. Phillips (1992), Paleoecology of late-glacial peats from the Bering Land Bridge, Chukchi Sea shelf region, northwestern Alaska, *Quat. Res.*, *38*, 371–378.
- Elias, S. A., S. K. Short, C. H. Nelson, and H. H. Birks (1996), Life and times of the Bering Land Bridge, *Nature*, *382*, 60–63.
- Gildor, H., and E. Tziperman (2000), Sea ice as the glacial cycles' climate switch: Role of seasonal and orbital forcing, *Paleoceanography*, *15*, 605–615.
- Hald, M., H. Ebbesen, M. Forwick, F. Godtlielsen, L. Khomenko, S. Korsun, L. Ringstad Olsen, and T. O. Vorren (2004), Holocene paleoceanography and glacial history of the West Spitsbergen area, Euro-Arctic margin, *Quat. Sci. Rev.*, *23*, 2075–2088.
- Hamel, D., A. de Vernal, M. Gosselin, and C. Hillaire-Marcel (2002), Organic-walled microfossils and geochemical tracers: Sedimentary indicators of productivity changes in the North Water and northern Baffin Bay (high Arctic) during the last centuries, *Deep Sea Res., Part II*, *49*, 5277–5295.
- Hebbeln, D., and G. Wefer (1991), Effects of ice coverage and ice-rafted material on sedimentation in the Fram Strait, *Nature*, *350*, 409–411.
- Hewitt, C. D., C. A. Senior, and J. F. B. Mitchell (2001), The impact of dynamic sea ice on the climatology and climate sensitivity of a GCM: A study of past, present, and future climates, *Clim. Dyn.*, *17*, 655–668.
- Hillaire-Marcel, C., A. de Vernal, G. Bilodeau, and A. J. Weaver (2001), Absence of deep water formation in the Labrador Sea during the last interglacial period, *Nature*, *410*, 1073–1077.
- Hillaire-Marcel, C., A. de Vernal, L. Polyak, and D. A. Darby (2004), Size-dependent isotopic composition of planktic foraminifers from Chukchi Sea vs. NW Atlantic sediments—Implications for the Holocene paleoceanography of the western Arctic, *Quat. Sci. Rev.*, *23*, 245–260.
- Hilmer, M., M. Harder, and P. Lemke (1998), Sea ice transport: A highly variable link between Arctic and North Atlantic, *Geophys. Res. Lett.*, *25*, 3359–3362.
- Hughen, K. A., et al. (2004), Marine radiocarbon age calibration, 0–26 cal. kyr BP, *Radiocarbon*, *46*, 1059–1086.
- Johannessen, O. L., E. V. Shalina, and M. W. Miles (1999), Satellite evidence for an Arctic sea ice cover transformation, *Science*, *286*, 1937–1939.
- Jones, E. P. (2001), Circulation in the Arctic Ocean, *Polar Res.*, *20*, 139–146.
- Jutterström, S., and L. G. Anderson (2005), The saturation of calcite and aragonite in the Arctic Ocean, *Mar. Chem.*, *94*, 101–110.
- Kaplan, J. O., et al. (2003), Climate change and Arctic ecosystems: 2. Modeling, paleo-data-model comparisons, and future projections, *J. Geophys. Res.*, *108*(D19), 8171, doi:10.1029/2002JD002559.
- Kaufman, D. K., et al. (2004), Holocene thermal maximum in the western Arctic (0–180°W), *Quat. Sci. Rev.*, *23*, 529–560.
- Kohfeld, K. E., R. G. Fairbanks, S. L. Smith, and I. D. Walsh (1996), *Neogloboquadrina pachyderma* (sinistral coiling) as paleoceanographic tracers in polar oceans: Evidence from Northeast Water Polynya plankton tows, sediment traps, and surface sediment, *Paleoceanography*, *11*, 679–699.
- Kunz-Pirrung, M. (1998), Rekonstruktion der Oberflächenwassermassen der östlichen Laptevsee im Holozän anhand von aquatischen Palynomorphen, *Ber. Polarforsch.* *281*, 117 pp., Alfred-Wegener-Inst. für Polar- und Meeresforsch., Bremerhaven, Germany.
- Kunz-Pirrung, M. (2001), Dinoflagellate cyst assemblages in recent sediments of the Laptev Sea (Arctic Ocean) and their relation to hydrographic conditions, *J. Quat. Sci.*, *16*, 637–650.
- Laxon, S., N. Peacock, and D. Smith (2003), High interannual variability of sea ice thickness in the Arctic region, *Nature*, *425*, 947–950.
- Mangerud, J., and S. Gulliksen (1975), Apparent radiocarbon ages of recent marine shells from Norway, Spitsbergen, and Arctic Canada, *Quat. Res.*, *5*, 263–273.
- Marshall, J., and F. Schott (1999), Open-ocean convection: Observations, theory, and models, *Rev. Geophys.*, *37*, 1–64.
- Marret, F. (1993), Les effets de l'acétolyse sur les assemblages de kystes de dinoflagellés, *Paly-nosciences*, *2*, 267–272.
- Mason, O. K., and J. W. Jordan (2002), Minimal late Holocene sea level rise in the Chukchi Sea: Arctic insensitivity to global change?, *Global Planet. Change*, *32*, 13–23.
- Matthiessen, J., J. Knies, N. R. Nowaczyk, and R. Stein (2001), Late Quaternary dinoflagellate cyst stratigraphy at the Eurasian continental margin, Arctic Ocean: Indications for Atlantic water inflow in the past 150,000 years, *Global Planet. Change*, *31*, 65–86.
- Moritz, R. E., C. M. Bitz, and E. J. Steig (2002), Dynamics of recent climate change in the Arctic, *Science*, *297*, 1497–1501.
- Mudie, P. J. (1992), Circum-arctic Quaternary and Neogene marine palynofloras: Paleoecology and statistical analysis, in *Neogene and Quaternary Dinoflagellate Cysts and Acritarchs*, edited by M. J. Head, and J. H. Wrenn, pp. 347–390, Am. Assoc. of Stratigr. Palynol. Found., College Station, Tex.
- Mudie, P. J., R. Harland, J. Matthiessen, and A. de Vernal (2001), Dinoflagellate cysts and high latitude Quaternary paleoenvironmental reconstructions: An introduction, *J. Quat. Sci.*, *16*, 595–602.
- Mudie, P. J., and A. Rochon (2001), Distribution of dinoflagellate cysts in the Canadian Arctic marine region, *J. Quat. Sci.*, *16*, 603–620.
- Mysak, L. A. (2001), Patterns of Arctic circulation, *Science*, *293*, 1269–1270.
- National Oceanographic Data Center (2001), *World Ocean Database 2001, Scientific Data Sets, Observed and Standard Level Oceanographic Data [CD-Rom]*, Natl. Oceanic and Atmos. Admin., Silver Spring, Md.
- Osterman, L. E., R. Z. Poore, and K. M. Foley (1999), Distribution of benthic foraminifers (>125 μm) in the surface sediments of the Arctic Ocean, *U.S. Geol. Surv. Bull.*, *2164*, 28 pp.
- Peterson, B. J., R. M. Holmes, J. W. McClelland, C. J. Vörösmarty, R. B. Lammers, A. I. Shiklomanov, I. A. Shiklomanov, and S. Rahmstorf (2002), Increasing river discharge to the Arctic Ocean, *Science*, *298*, 2171–2173.
- Polyakova, Y. I., H. A. Bauch, and T. S. Klyuytkina (2005), Early to middle Holocene changes in Laptev Sea water masses deduced from diatom and aquatic palynomorph assemblages, *Global Planet. Change*, *48*, 208–222.
- Poore, R. Z., L. Osterman, W. B. Curry, and R. L. Phillips (1999), Late Pleistocene and Holocene meltwater events in the western Arctic Ocean, *Geology*, *27*, 759–762.
- Radi, T., and A. de Vernal (2004), Dinocyst distribution in surface sediments from the northeastern Pacific margin (40–60°N) in relation to hydrographic conditions, productivity and upwelling, *Rev. Palaeobot. Palynol.*, *128*, 163–193.
- Radi, T., A. de Vernal, and O. Peyron (2001), Relationships between dinocyst assemblages in surface sediment and hydrographic conditions in the Bering and Chukchi seas, *J. Quat. Sci.*, *16*, 667–680.
- Rigor, I. G., J. M. Wallace, and R. L. Colony (2002), On the response of sea ice to the Arctic Oscillation, *J. Clim.*, *15*, 2546–2663.
- Rudels, B., E. P. Jones, L. G. Anderson, and G. Kattner (1994), On the intermediate depth water in the Arctic Ocean, in *The Role of Polar Oceans in Shaping the Global Climate*, *Geophys. Monogr. Ser.*, vol. 85, edited by O. M. Johannessen et al., pp. 33–46, AGU, Washington, D. C.
- Sarnthein, M., S. Van Kreveld, H. Erlenkeuser, P. M. Grootes, M. Kucera, U. Pflaumann, and M. Schulz (2002), Centennial-to-millennial-scale periodicities of Holocene climate and sediment injections off the western Barents shelf, 75°N, *Boreas*, *32*, 447–461.
- Schmidt, G. A. (1999), Forward modeling of carbonate proxy data from planktonic foraminifera using oxygen isotope tracers in a global ocean model, *Paleoceanography*, *14*, 482–497.
- Solignac, S., A. de Vernal, and C. Hillaire-Marcel (2004), Holocene sea-surface conditions in the North Atlantic—Contrasted trends and regimes in the western and eastern sectors (Labrador Sea vs. Iceland Basin), *Quat. Sci. Rev.*, *23*, 319–334.
- Spero, H. J., and D. W. Lea (1996), Experimental determination of stable isotope variability in *Globigerina bulloides*: Implications for paleoceanographic reconstructions, *Mar. Micropaleontol.*, *28*, 231–246.
- Stein, R., et al. (2004), Arctic (palaeo) river discharge and environmental change: Evidence from the Holocene Kara Sea sedimentary record, *Quat. Sci. Rev.*, *23*, 1485–1511.
- Stuiver, M., and P. J. Reimer (1993), Extended ¹⁴C data base and revised CALIB 3.0 ¹⁴C age calibration program, *Radiocarbon*, *35*, 215–230.
- Stuiver, M., P. J. Reimer, E. Bard, J. W. Beck, G. S. Burr, K. A. Hughen, B. Kromer, G. McCormick, J. van der Plicht, and M. Spurk (1998), Radiocarbon age calibration, 24,000–0 cal. BP, *Radiocarbon*, *40*, 1041–1083.
- Vavrus, S., and S. P. Harrison (2003), The impact of sea ice dynamics on the arctic climate system, *Clim. Dyn.*, *20*, 741–757.
- Vinnikov, K. A., A. Robock, R. J. Stoufer, J. E. Walsh, C. L. Parkinson, D. J. Cavalieri, J. F. B. Mitchell, D. Garrett, and V. F. Zakharov (1999), Global warming and Northern Hemi-

- sphere Sea ice extent, *Science*, 286, 1934–1937.
- Voronina, E., L. Polyak, A. de Vernal, and O. Peyron (2001), Holocene variations of sea-surface conditions in the southeastern Barents Sea based on palynological data, *J. Quat. Sci.*, 16, 717–727.
- Walsh, J. E., and W. L. Chapman (2001), Twentieth-century sea-ice variations from observational data, *Ann. Glaciol.*, 33, 444–448.
- Weatherly, J. W., and J. E. Walsh (1996), The effects of precipitation and river runoff in a coupled ice-ocean model of the Arctic, *Clim. Dyn.*, 12, 785–798.
- Weingartner, T., K. Aagard, R. Woodgate, S. Danielson, Y. Sasaki, and D. Cavalieri (2005), Circulation on the North Central Chukchi Sea Shelf, *Deep Sea Res., Part II*, in press.
- Wolfe, B. B., T. W. D. Edwards, R. Aravena, S. L. Forman, B. G. Warner, A. A. Velichko, and G. M. MacDonald (2000), Holocene paleohydrology and paleoclimate at treeline, north-central Russia, inferred from oxygen isotope records in lake sediment cellulose, *Quat. Res.*, 53, 319–329.
- Zonneveld, K. A., G. H. Versteegh, and G. J. de Lange (2001), Paleoproductivity and post-depositional aerobic organic matter decay reflected by dinoflagellate cyst assemblages in eastern Mediterranean S1 sapropel, *Mar. Geol.*, 172, 181–195.

D. A. Darby, Department of Ocean, Earth, and Atmospheric Sciences, Old Dominion University, 4600 Elkhorn Avenue, Norfolk, VA 23529-0276, USA.

A. de Vernal and C. Hillaire-Marcel, Centre de Recherche en Géochimie et en Géodynamique, Université du Québec à Montréal, CP 8888, Succursale Centre Ville, Montréal, Québec, Canada H3C 3P8. (devernal.anne@uqam.ca)

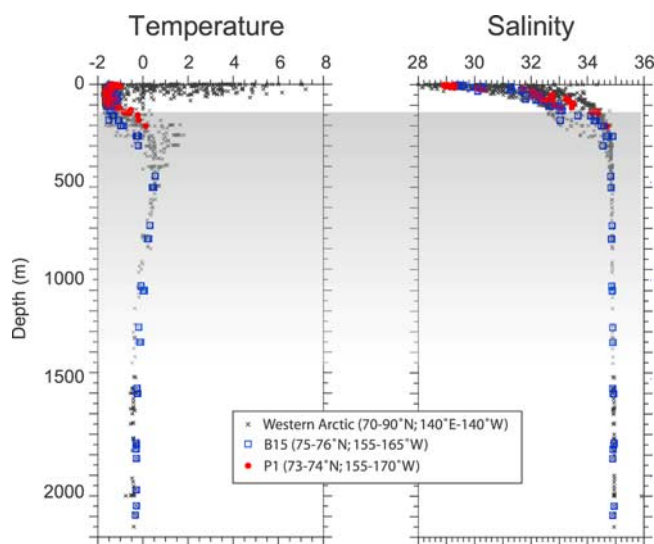


Figure 2. Temperature and salinity versus depth in the water column of the western Arctic Ocean (grey symbols correspond to measurements between 140°E and 140°W and from 70° to 90°N) and around coring sites (B15, blue symbols; P1, red symbols). The data are from the Goddard Institute database (available at <http://www.giss.nasa.gov/data/o18data/> [cf. Schmidt, 1999; Bigg and Rohling, 2000]). The grey horizon corresponds to the North Atlantic water mass below the cold and low-saline surface Arctic water layer.

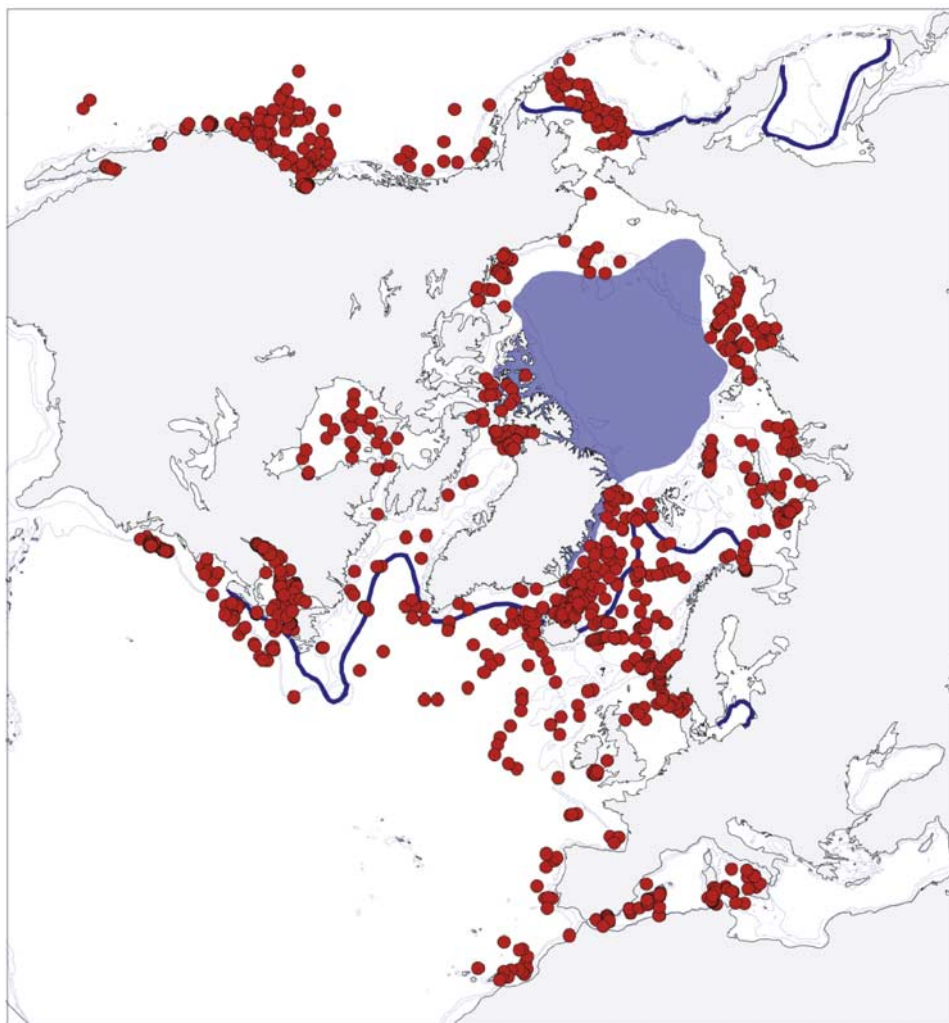


Figure 4. Map showing the location of surface sediment samples used to develop the reference dinocyst database ($n = 1054$). The minimum and maximum sea ice cover extents are shown by the blue zone and the blue line, respectively. The database includes assemblages for 516 sites characterized by seasonal sea ice, about half of them corresponding to more than 6 months per year of sea ice. It is important to mention that many other samples collected under the perennial pack ice of the Arctic Ocean revealed barren assemblages. These samples are not included in the database. In the Arctic Ocean context, barren dinocyst assemblages are associated with nil cyst fluxes because of extremely low productivity.

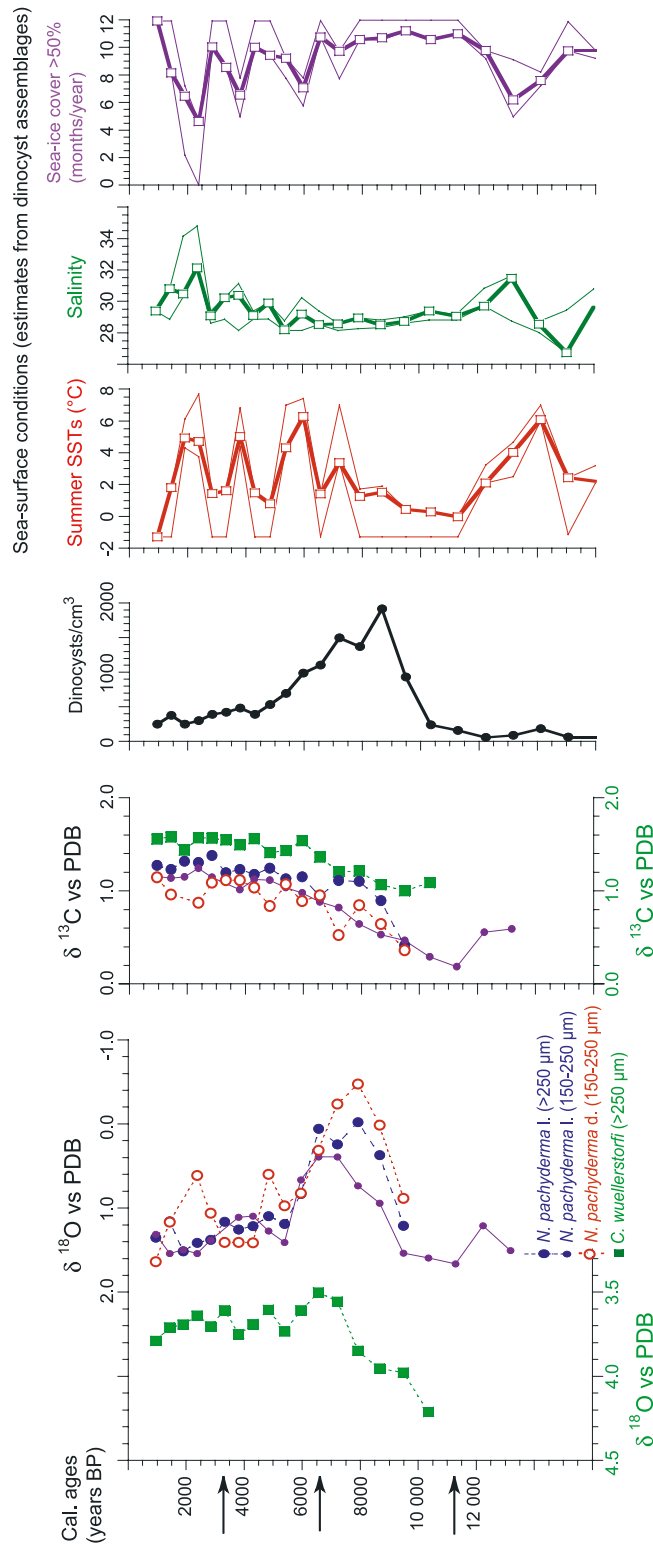


Figure 7. Isotopic data ($\delta^{18}\text{O}$ and $\delta^{13}\text{C}$) of benthic and planktonic foraminifer shells hand-picked in different size fractions, dinocyst concentrations, and estimates of sea surface conditions based on dinocyst assemblages in the archive core B15. The squares correspond to the best estimates, which are the averages weighted inversely to the distance for the five best modern analogues (for details, see *de Vernal et al.* [2001]). The thin lines correspond to the minimum and maximum values possible according to the set of five analogues. The vertical scale is the calibrated age as interpolated from the three age controls shown by arrows.